



Fundamentals and Recent Trends in Microwave Oscillators

*Nikolay Shtin^{ID}, Suresh Ojha^{ID},
Alexander Chenakin^{ID}, and Paul Khanna^{ID}*

An oscillator is considered a key element of any modern wireless system. Microwave oscillators in particular are commonly used as local oscillators in a number of applications, such as wireless communication transceivers, test and measurement equipment, radars, wireless sensors, among others.

Introduction

Since the oscillator performance has a direct impact on the system characteristics, rapidly growing and

evolving wireless systems have a constant demand for oscillator performance improvements. Modern wireless communication systems require higher data rates and increased performance. These requirements demand improvements in key oscillator parameters, such as operating frequency range and phase noise, to support high-order modulation schemes and multiple operating frequency bands, which now extend into the millimeter-wave spectrum. On the other hand, the ceaseless demand for wireless equipment miniaturization and improved power efficiency has led to increasing requirements on the oscillator form factor and its power efficiency. Aerospace and military applications also require oscillators to maintain their performance under extreme environmental conditions and provide a good level of immunity to external disturbances, such as vibration, radiation, etc. Moreover, some emerging applications, such as quantum computing, require chip-scale oscillators that must reliably operate at

Nikolay Shtin (nikolay.shtin@anritsu.com), Suresh Ojha (suresh.ojha@anritsu.com), and Alexander Chenakin (alexander.chenakin@anritsu.com) are with Anritsu Company, Morgan Hill, CA 95037 USA. Paul Khanna (paul@apionics.us) is with Apionics, LLC, San Jose, CA 95124 USA.

*Digital Object Identifier 10.1109/MMM.2025.3538559
Date of current version: 7 April 2025*

cryogenic temperatures and provide excellent performance in terms of phase noise and ultralow power consumption. Today, microwave oscillators used in commercial communication systems are implemented using monolithic microwave integrated circuit (MMIC) or RFIC technologies, which enable a very high level of device integration. Some applications, such as test and measurement equipment, continue to employ high-performance microwave oscillators that can use a number of technologies, including MMICs, hybrid circuits, and photonics as well as conventional electronic and RF circuits. In this article, we present a review of the microwave oscillator design trends and technology advances made in about the past 20 years with an emphasis on state-of-the-art low-noise oscillators. We also present some relevant discussions on design techniques that may help provide a better insight into oscillator optimization for improved phase noise performance.

Negative Resistance Oscillator

The negative resistance oscillator, also known as the *Kurokawa oscillator*, is by far the most widely used microwave oscillator design [1]. Sometimes, it is also referred to as a reflection oscillator. A diagram of the negative resistance oscillator is presented in Figure 1. In this approach, the active device is represented by the nonlinear admittance $Y_d(V)$, which is a function of the voltage across the device terminals. The device admittance has a negative real part $-G_d$ that is achieved through the use of a positive feedback introduced into the active device circuit, or it can be an intrinsic property of the device itself, as in the case of tunnel and Gunn diodes. The oscillator also contains a linear load represented by the frequency-dependent admittance $Y_L(\omega)$ connected in parallel to the device. In this case, the linear load represents the resonator, which can be coupled to the active device input or output. The oscillation condition for this network is given by

$$Y_L(\omega) + Y_D(A) = 0 \quad (1)$$

where A is the first-harmonic amplitude.

The same condition can be expressed in terms of the reflection coefficients:

$$\Gamma_{in}(A, \omega)\Gamma_L(\omega) = 1. \quad (2)$$

It is worth mentioning that modern CAD tools employ a special probe component, shown in Figure 2, that allows one to generate an open-loop circuit at the fundamental frequency and keep the loop closed at the harmonic frequencies. In this case, the open-loop gain can be expressed as [2]

$$\frac{b_3}{a_4} = \Gamma_{in}(A, \omega)\Gamma_L(\omega). \quad (3)$$

Once the probe is placed into the oscillator circuit, a harmonic balance simulator is used to perform a

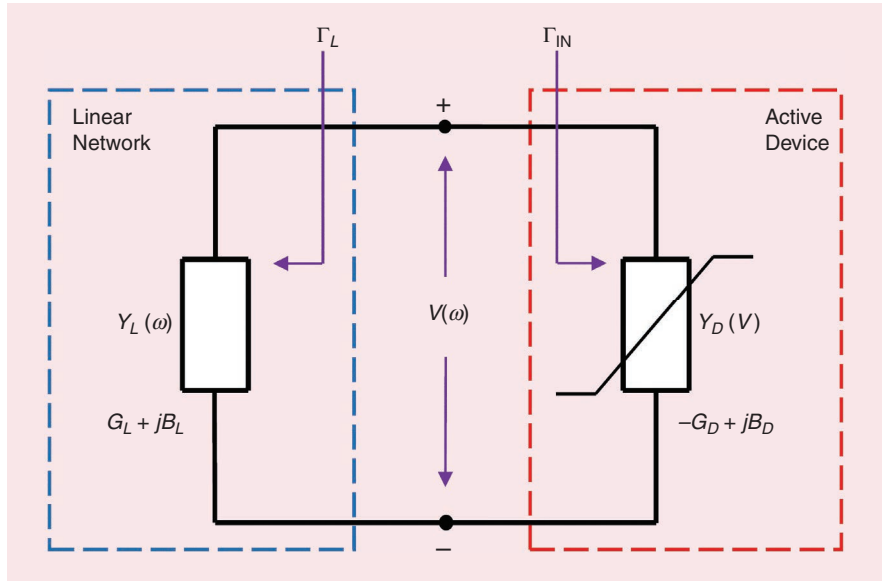


Figure 1. Negative resistance oscillator.

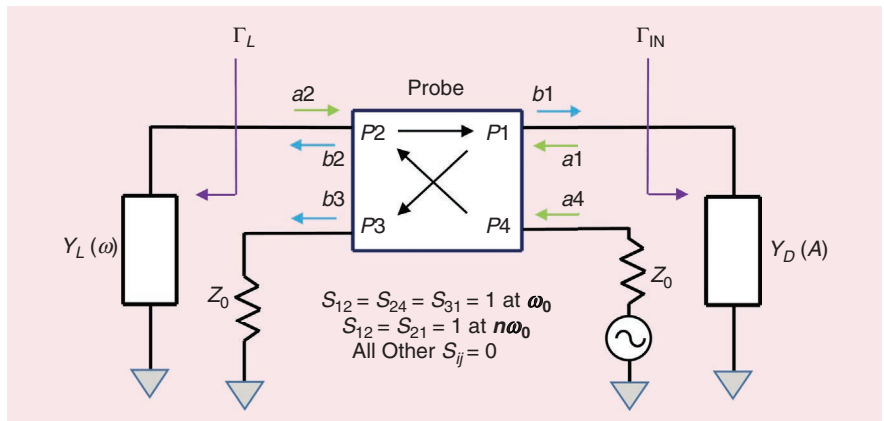


Figure 2. Negative resistance oscillator with open-loop probe.

simultaneous A and ω sweep to determine the oscillator operating point. In fact, the same type of auxiliary probe component can also be employed in a linear oscillator analysis to predict a tentative oscillation frequency satisfying the following start-up conditions:

$$|\Gamma_{in}(A, \omega)\Gamma_L(\omega)| \geq 1 \quad (4a)$$

$$\angle(\Gamma_{in}(A, \omega)\Gamma_L(\omega)) = 0. \quad (4b)$$

We note that the negative resistance approach is widely used in the design of integrated and broadband oscillators as well as oscillators based on one-port active devices. However, the main drawback of this technique is the difficulty in accurately estimating the resonator loaded Q-factor, which is one of the key oscillator parameters strongly related to the phase noise.

Feedback Oscillator

A block diagram of the feedback oscillator is presented in Figure 3. In this oscillator model, the active device represented, for example, by an amplifier is connected to the positive feedback network comprising a resonator

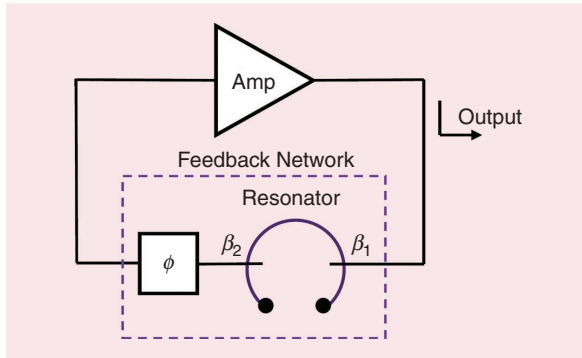


Figure 3. Feedback microwave oscillator.

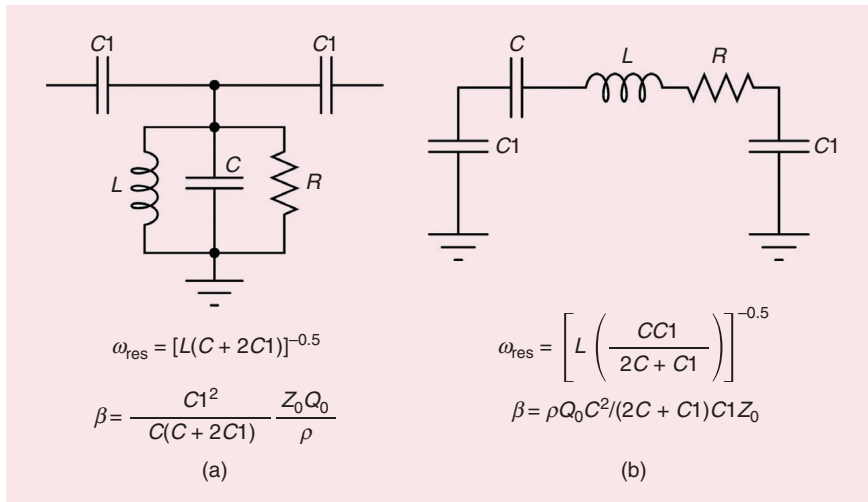


Figure 4. Lumped element two-port resonators.

and a phasing network. This model is especially well suited for oscillators employing amplifiers with 50- Ω input and output impedances and transmission-type resonators. These types of resonators are very common at microwave frequencies; they use a high-Q resonant structure coupled to the input and output transmission lines. The strength of the coupling is defined using the input and output coupling coefficients β_1 and β_2 . As shown in Figure 4, this type of resonator can also be implemented using the lumped series or parallel tank circuits commonly used in LC oscillators [3]. Note that, in the case of equal couplings at the input and output of the resonator, its S_{21} response or the voltage transfer function is given by

$$S_{21}^{\text{res}} = \frac{2\beta}{1 + 2\beta + j2Q_0 \left(\frac{f - f_{\text{res}}}{f_{\text{res}}} \right)} \quad (5)$$

where β is the coupling coefficient and Q_0 is the unloaded Q-factor of the resonator. In the case of the mentioned series and parallel tank resonators, one may expect them to have identical loaded Q-factors, $Q_L = Q_0 / (1 + 2\beta)$, and insertion losses, $L = (1 + 2\beta)^2 / 4\beta^2$. However, notably, the input and output impedances of the series tank circuit are lower compared to the parallel tank ones by a factor of $(1 + \beta)^2 / \beta^2$. Thus, the series tank resonator generally results in a lower phase noise because its low impedance helps to reduce the impact of thermal noise and other noise sources within the oscillator circuit.

For the feedback oscillator analysis, a special auxiliary probe, as shown in Figure 5, can be employed [3]. This probe is somewhat similar to the previously introduced open-loop probe used for the negative resistance oscillator analysis, and it allows one to break the oscillation loop in the forward direction while keeping it closed for the reflected signal. Using the probe S-parameter matrix given at the fundamental frequency, one may obtain the expression for the feedback oscillator open-loop gain:

$$G_{OL} = \frac{b_4}{a_3} = S_{21} + \frac{S_{11}S_{22}}{1 - S_{12}} \quad (6)$$

where S_{ij} are the S-parameters of the open-loop network. It is noteworthy that, according to (6), G_{OL} may increasingly deviate from S_{21} when S_{12} of the amplifier as well as the reflections from the resonator increase. Expression (6) can be used to establish the oscillator's well-known start-up conditions, requiring, at the oscillation frequency, that the

loop gain must be greater than unity, and the phase shift around the loop must be an integer multiple of 2π radians. Employing these conditions, the oscillation frequency can be found by performing an analysis of the open-loop circuit and finding the frequency at which the phase of the open-loop response is zero. The open-loop gain at the given frequency is also an important parameter, referred to as the *oscillator gain margin*. For a reliable oscillation, a gain margin of at least 3 dB is recommended.

Moreover, the loaded Q-factor can be found by analyzing the group delay τ of the open-loop response. In the case of a simple single-tank resonator, the loaded Q-factor and group delay are related by $Q_L = \omega\tau/2$.

Thus, the analysis of the feedback oscillator open-loop response allows one to accurately determine most important oscillator parameters, such as the oscillation frequency, the gain margin, and the loaded Q-factor. One of the important details of this method is that the characteristic impedance of the probe must be set equal to the input impedance of the loop amplifier; otherwise, one may get inaccurate simulation results.

Oscillator Phase Noise

Phase noise is one of the key oscillator parameters that describe the spectral purity of its output signal. Oscillator phase noise originates in a parasitic modulation of the carrier signal by the noise produced in the oscillator's electronics. Phase noise is typically defined in the frequency domain, and it is expressed in terms of the double-sideband power spectral density $S_\phi(f)$ [dBc/Hz] representing the noise power relative to the carrier contained in a 1-Hz bandwidth centered at a certain offset from the carrier. Along with $S_\phi(f)$, it is common to characterize the phase noise by its single-sideband power spectral density $\mathcal{L}(f) = S_\phi(f)/2$.

The first simple semiempirical phase noise model was proposed by Leeson [4]. According to this model, the phase noise spectral density of an LC oscillator can be expressed as

$$S_\phi(f_m) = S_{\Delta\theta}(f_m) \left(1 + \left(\frac{f_0}{2f_m Q_L} \right)^2 \right) \quad (7)$$

where f_m is the offset from the carrier frequency, f_0 is the oscillation frequency, Q_L is the resonant tank loaded Q-factor, and $S_{\Delta\theta}(f_m)$ is the spectral density of the oscillator input phase uncertainty associated with the intrinsic noise of the active device [5]:

$$S_{\Delta\theta}(f_m) = b_0 + \frac{b_{-1}}{f_m} \quad (8)$$

where b_0 is the additive white noise component, which in the case of an active device with noise figure NF is given by

$$b_0 = \frac{k_B T N F}{P_{in}} \quad (9)$$

where k_B is the Boltzmann constant, T is the ambient temperature, and P_{in} is the power of the signal at the input of the active device. Meanwhile, the second term in (8) represents $1/f$ or the flicker noise. Note that, unlike for b_0 , the value of b_{-1} is independent of the carrier power that is related to the $1/f$ noise parametric origin [5]. Strictly speaking, this is a true statement only when the active device operates in the small-signal or weak compression regimes. Under large-signal conditions (strong compression), some active devices may present variations in their $1/f$ noise and also exhibit the noise figure degradation that results from different nonlinear phenomena [e.g., dc bias changes, amplitude-to-phase modulation (AM/PM) conversion, etc.] [6], [7].

Combining equations (8) and (9), one may find the frequency at which the white noise and the $1/f$ noise terms are equal:

$$f_C = \frac{b_{-1}}{k_B T N F} P_{in}. \quad (10)$$

This frequency is known as the flicker noise corner frequency f_C , and it is often used as a figure of merit (FoM) for active devices, amplifiers, and oscillators. Active devices based on different semiconductor technologies may exhibit very different levels of $1/f$ noise and, thus, f_C . The most widely used devices allowing one to achieve a low f_C are the heterojunction bipolar transistors (HBTs), which are available in several technologies, such as SiGe, AlGaAs/GaAs, and InGaP/GaAs HBTs. The HBTs are, in general, preferred over the other active devices, essentially because of their low-frequency (LF) noise, which can be up to two orders of magnitude lower compared to that of the GaAs field-effect devices [10].

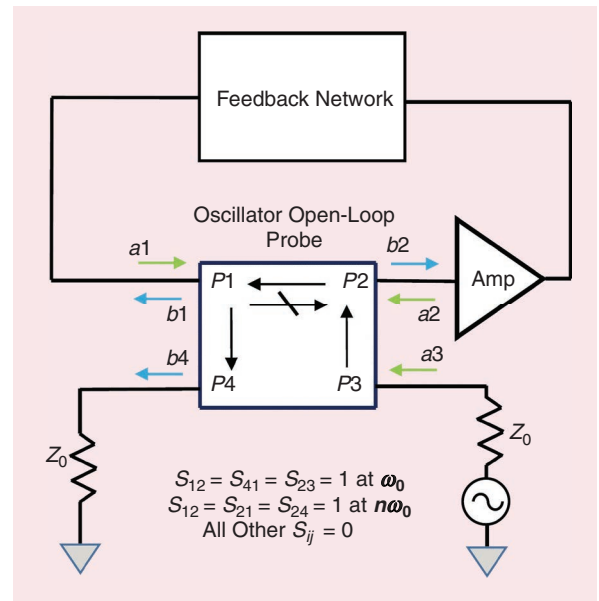


Figure 5. Feedback oscillator with open-loop probe.

A typical oscillator phase noise spectrum described by the Leeson model is shown in Figure 6. As one may see, apart from the white and flicker noise, the oscillator spectrum may also contain random-walk fluctuations that have an f^{-4} slope and can be associated with frequency fluctuations due to temperature variations as well as to the intrinsic resonator noise.

A more comprehensive oscillator phase noise model has been proposed by Rubiola [8]. This model is based on the linear feedback oscillator approach, and it manipulates the oscillator loop phase noise using Laplace transforms. To describe the oscillator feedback network, it employs a phase transfer function that allows one to calculate phase noise at the oscillator output from the phase fluctuations introduced by the active device. Thus, in this model, the phase noise spectral density at the oscillator output can be expressed as

$$S_{\phi}(f_m) = S_{\phi}^{\text{amp}}(f_m) |H(f_m)|^2 \quad (11)$$

where $H(f_m)$ is the phase transfer function of the oscillator closed loop given by

$$H(f_m) = \frac{1}{1 - B(jf_m)} \quad (12)$$

where $B(jf_m)$ is the open-loop phase transfer function, which can be computed from the open-loop gain response using the known relation between $B(f_m)$ and the ordinary transfer function of the linear network [8]:

$$B(j2\pi f_m) = \frac{G_{OL}(j2\pi(f_0 + f_m)) + G_{OL}(j2\pi(-f_0 + f_m))}{2G_{OL}(j2\pi f_0)} \quad (13)$$

Note that, by making use of (12) and (13), it can be shown that for a single-tank resonator with the

frequency response given by (5), the closed-loop phase transfer function becomes

$$H(f_m) = 1 + \frac{1}{j f_m 2 Q_L / f_0} \quad (14)$$

where $Q_L = Q_0 / (1 + 2\beta)$. Substitution of (14) into (11) yields a phase noise expression identical to the Leeson formula (7). In fact, taking into account that $P_{\text{in}} = P_{\text{out}} (|S_{21}^{\text{res}}|^2)$, (7) can be written as follows:

$$S_{\phi}(f_m) = \left[\frac{k_B T N F}{P_{\text{out}}} \left(\frac{1 + 2\beta}{2\beta} \right)^2 + \frac{b_{-1}}{f_m} \right] \left\{ 1 + (1 + 2\beta)^2 \left(\frac{f_0}{2 f_m Q_0} \right)^2 \right\} \quad (15)$$

where P_{out} is the active device output power. Moreover, assuming that the signal-to-noise ratio $k_B T N F / P_{\text{out}}$ is independent of the active device input power, it can be shown that the phase noise in the f^{-2} region is minimized when $\beta = 0.5$ or $Q_L = Q_0 / 2$. In this case, (15) becomes

$$S_{\phi}^{\text{min}}(f_m) = \left[\frac{4 k_B T N F}{P_{\text{out}}} + \frac{b_{-1}}{f_m} \right] \left\{ 1 + \left(\frac{f_0}{f_m Q_0} \right)^2 \right\} \quad (16)$$

We point out that the active device noise figure used in (15) and (16) corresponds to the large-signal regime and may differ significantly from the conventional transistor noise figure measured under small-signal conditions. Thus, in [6] it has been shown that low-noise bipolar junction transistors (BJTs) may exhibit a considerable increase in their noise figure at power levels beyond the device 1-dB compression point (P1dB). On the other hand, GaAs pseudomorphic high-electron mobility transistor (pHEMT) devices operating beyond P1dB were proved to have fairly weak NF dependence on the input power [7]. However, as mentioned earlier, the GaAs pHEMT devices typically exhibit much higher levels of $1/f$ noise as well as a pronounced generation-recombination noise [11], so they are rarely used in low-phase-noise oscillators. To reduce the active device noise, in some works it has been proposed to utilize a diode limiter or an automatic amplitude control loop that would help to keep the amplifier in the linear regime [9].

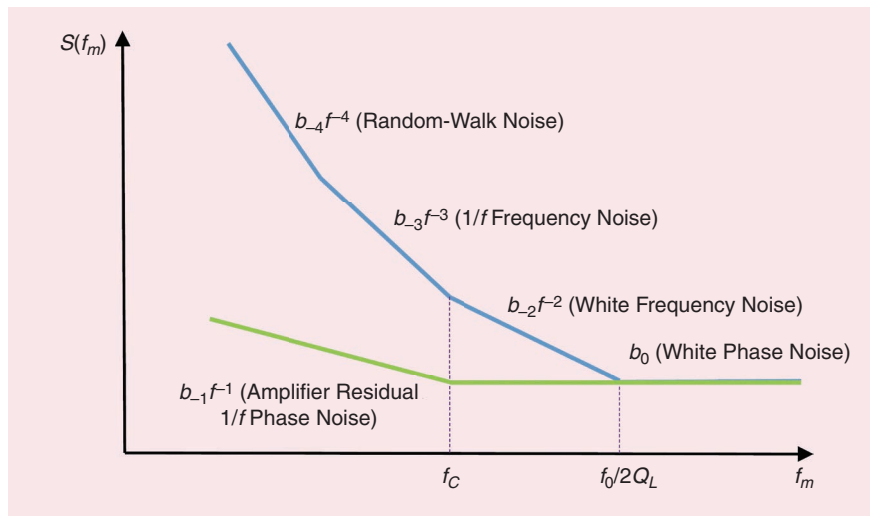


Figure 6. Typical phase noise spectrum of a microwave oscillator.

It is important to note that, to reduce $1/f$ noise upconversion, an active device must be operated at the bias point, where a small S_{21} phase sensitivity to the bias current is observed [5]. Moreover, it is essential to provide a clean oscillator supply voltage using a low-noise linear voltage regulator. Apart from that, to reduce the LF noise, it is recommended to use passive bias networks, preferably those having low impedance at low frequencies.

TABLE 1. Comparison of high-Q resonator technologies.

Resonator Technology	Typical Frequency Range, GHz	Q-Factor	Q·f, GHz
SAW	0.25–1.6	5,000–15,000 ¹	12,000 ¹
FBAR	0.3–3	500–2,000	>4,000 [16]
HBAR	0.3–4	26,000–53,000	79,500 [19]
Coaxial resonator	0.3–6	70–1,320	4,900 ³
DR	1.5–40	1,200–35,000 ²	430,000 [23]
SLC @ 300 K	4.5–20	100,000–350,000	$1.8 \cdot 10^6$ [29], [32]

¹Commercially available SAW resonators (TAI-SAW Technology Co., Ltd.).
²Commercially available DRs (www.exxelia.com).
³Commercially available ceramic coaxial resonators (www.trans-techinc.com).
SAW: surface acoustic wave; FBAR: film bulk acoustic resonator; HBAR: high-overtone bulk acoustic resonator; SLC: sapphire loaded cavity; DR: dielectric resonator.

Oscillator FOM

Note that there are always tradeoffs between the oscillator phase noise and other parameters, such as power efficiency, output power, and frequency tuning range (FTR). Additionally, in accordance with the Leeson formula, the phase noise increases with the square of the oscillator frequency. Given this situation, it is customary to benchmark microwave oscillators in terms of the FoM, which accounts for the mentioned design tradeoffs and takes into account the oscillator operating frequency. The most frequently used FoM definition accounts for the tradeoff between the phase noise and the dc power consumption as well as the oscillator frequency f_{osc} and it is given by

$$FoM = \left(\frac{f_{osc}}{f_m} \right)^2 \frac{1}{P_{dc} \mathcal{L}(f_m)} \quad (17)$$

where $\mathcal{L}(f_m)$ is the single-sideband phase noise power spectral density and P_{dc} is the power consumption in milliwatts. FoM is measured in inverse watts, and it is often expressed in decibels (or dBc/Hz) relative to 1 mW. Another form of FoM that includes the oscillator output power is given by

$$FoM_P = \left(\frac{f_{osc}}{f_m} \right)^2 \frac{P_{out}}{P_{dc} \mathcal{L}(f_m)}. \quad (18)$$

FoM_P is often used for oscillators operating at millimeter-wave frequencies, where a difficulty in generating a sufficiently high output power may exist.

Another widely used definition of FoM that takes into account both P_{dc} and the FTR is given by

$$FoM_T = \left(\frac{f_{osc}}{f_m} \right)^2 \left(\frac{FTR}{10} \right)^2 \frac{1}{P_{dc} \mathcal{L}(f_m)} \quad (19)$$

where $FTR = 100(f_{max} - f_{min}) / ((1/2)(f_{max} + f_{min}))$, with f_{min} and f_{max} being, respectively, the minimum and maximum oscillator frequencies. We note that FoM_T is normalized to the 10% tuning range that is a typical requirement in some wireless systems.

Ultimately, in some applications where dc power consumption is not critical and the oscillator operates at a fixed frequency, another simplified form of FoM independent of power and FTR can be used:

$$FoM_{PN} = \left(\frac{f_{osc}}{f_m} \right)^2 \frac{1}{\mathcal{L}(f_m)}. \quad (20)$$

In general, to achieve an excellent FoM, it is essential to both reduce the oscillator phase noise and increase the dc-to-RF conversion efficiency. The preceding FoM_{PN} definition is clearly more favorable for oscillators, whose phase noise can be reduced by increasing P_{dc} for example, by using multiple parallel active devices or multiple coupled oscillators.

Single-Frequency Oscillators

Single-frequency oscillators (SFOs) are used to provide a microwave signal at one particular fixed frequency. In some applications, SFOs are required to have a narrow-band frequency tuning that typically does not exceed the 3-dB bandwidth of their resonant tank circuit. The main requirements for this type of oscillator are high spectral purity (i.e., low phase noise) and good frequency stability. SFOs are built using high-Q resonators, which can be based on a number of technologies depending on the oscillator requirements, such as phase noise, frequency stability, form factor, etc. Table 1 shows the main resonator technologies with their basic characteristics, including frequency range, Q-factor, and best reported Qf product, which is frequently used to benchmark different types of resonators.

Acoustic wave-based devices, including surface acoustic wave (SAW) resonators, film bulk acoustic resonators (FBARs), and high-overtone bulk acoustic resonators (HBARs) are very attractive choices for microwave oscillator implementation because of their high Q-factor, small size, and low sensitivity to environmental factors and vibrations. The maximum operating frequency of the acoustic wave devices typically does not exceed several gigahertz, while the Q-factor

ranges from 1,000 to 2,000 in the case of FBARs [15], [16] and can reach 51,000 for HBAR devices [19].

SAW resonators are the most commonly utilized types of acoustic devices for oscillator design in the 0.3–3-GHz frequency range. Because of the high Q -factor [12], [13], typical SAW-based oscillators operating below 1 GHz exhibit quite a low phase noise, close to -150 dBc/Hz at 10-kHz offset [13]. SAW oscillators operating above 1 GHz (typically at 2.4–2.5 GHz) are reported to have phase noise in the vicinity of -130 dBc/Hz at 10-kHz offset [14]. Some commercial state-of-the-art SAW oscillators achieve quite remarkable phase noise values; for example, the Rakon 1-GHz oscillator (LNO 1000 D1) exhibits a phase noise as low as -159 dBc/Hz at 10 kHz.

The phase noise of the FBAR-based oscillators can be 10 to 30 dB higher when compared to the SAW oscillators [16], [17]. However, FBAR technology allows the implementation of chip-scale oscillators by integrating the FBAR into the active-circuit chip [16]. Interestingly, Imani and Hashemi [18] reported an integrated 1.5-GHz FBAR-based frequency discriminator (FD) and a phase noise suppression system using $0.13\text{-}\mu\text{m}$ CMOS technology. In this approach, the authors were able to achieve a phase noise of -128 dBc/Hz at 20-kHz offset and a noise floor of -166 dBc/Hz. Notably, integrated bulk acoustic resonators find a use in several of the latest Texas Instruments products (e.g., LMK05318), which utilize a voltage-controlled bulk acoustic wave oscillator (VCBO) operating at about 2.5 GHz. The VCBOs exhibit a phase noise close to -130 dBc/Hz at 100-kHz offset and outperform state-of-the-art integrated LC oscillators by approximately 10 dB.

HBARs based on an AlN-sapphire structure offer the highest Q -factor (typically 19,000–25,000) among all of the acoustic wave devices. Such a high Q_0 makes the HBARs excellent candidates for low-noise microwave and RF oscillators. Thus, HBAR-based low-noise oscillators operating at around a 2-GHz frequency and exhibiting phase noise values as low as -120 dBc/Hz at 1-kHz offset were reported by Boudot et al. [20]. Apart from their low phase noise, HBAR-based oscillators were also proved to have an excellent short-term frequency stability, which makes them well suited for atomic clock applications [21].

It is worth noting that the phase noise performance of the oscillators based on all types of acoustic wave resonators was found to be limited by the intrinsic resonator $1/f$ noise and linearity [13], [20].

Another type of resonator finding very broad application in RF and microwave oscillators is based on low-loss microwave ceramics. Thus, ceramic coaxial resonators are widely used at the low end of the microwave spectrum ($f < 6$ GHz). The unloaded Q -factor of the commercial coaxial resonators typically ranges

from approximately 200 to 1,000, depending on the ceramic material and the resonator size. According to the results presented in [22], coaxial resonator oscillators (CROs) may achieve a phase noise comparable to that of the SAW-based oscillators. For a 2.488-GHz CRO, it can be as low as -123 dBc/Hz at 10-kHz offset, while a 1-GHz CRO proved to have a phase noise better than -130 dBc/Hz at the same 10-kHz offset.

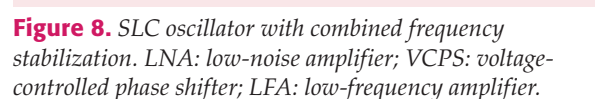
Another widely used type of ceramic resonator is the $\text{TE}_{01\delta}$ -mode cylindrical or disk dielectric resonator (DR). High- Q DRs are made using low-loss ceramic materials that typically have a high dielectric constant ϵ_r and a low temperature coefficient of frequency τ_f . The ceramics exhibiting the lowest dielectric losses are based on $\text{Ba}(\text{Mg}_{1/3}\text{Ta}_{2/3})\text{O}_3$ (BMT) or $\text{Ba}(\text{Zn}_{1/3}\text{Ta}_{2/3})\text{O}_3$ (BZT) composites. Thus, for BMT, $\epsilon_r = 24$, $Qf = 240,000\text{--}430,000$ GHz, and $\tau_f = 1\text{--}5$ ppm/ $^\circ\text{C}$, while BZT (with dopants) has $\epsilon_r = 28\text{--}30$ and can reach $Qf = 140,000\text{--}210,000$ GHz and $\tau_f = 0\text{--}1$ ppm/ $^\circ\text{C}$ [23]. There are other types of low-loss microwave ceramics, e.g., $\text{BaO-TiO}_2\text{-WO}_3$ and $(\text{Zr},\text{Sn})\text{TiO}_4$, with higher dielectric constants ($\epsilon_r = 34\text{--}38$) that also exhibit quite high Qf values of $40,000\text{--}70,000$ GHz and close to zero τ_f [23]. Currently, commercially available DRs cover the 1–40-GHz frequency range and offer Qf values that range approximately from 10,000 to 230,000. These resonators, because of their exceptionally high Q -factors and compact size, are perfect candidates for low-noise microwave oscillator implementation. To date, DR oscillators (DROs) remain one of the best solutions in terms of phase noise and frequency stability. Apart from that, DROs can be designed to have a fairly small form factor as well as low cost. The best phase noise results for this type of oscillator were reported in [24] and [25]. Everard and Theodoropoulos achieved a remarkably low phase noise of -170 dBc/Hz at 10-kHz offset for a 1.25-GHz DRO [24]. Meanwhile, Deshpande and Everard reported a 3.8-GHz DRO based on the feedback oscillator topology with phase noise of -150 dBc/Hz at 10-kHz offset using a DR with $Q_0 = 30,000$ and a low-noise push-pull amplifier [25]. Another low-noise X-band DRO with wide frequency tuning and a phase noise of -135 dBc/Hz at 10-kHz offset based on a BaTiO_3 DR with $Q_0 = 30,000$ and an SiGe HBT amplifier was reported by Sallin et al. [26]. We mention that Florian et al. reported a 7.61-GHz DRO having a similar low phase noise of -135 dBc/Hz at 10-kHz offset using a DR with a significantly lower Q -factor ($Q_0 = 8,800$) [27]. Their design is based on the series feedback topology and employs a medium-power InGaP HBT with low intrinsic LF noise.

An original low-noise DRO operating at a higher frequency of 174 GHz was proposed by Xia et al. [28]. Their approach utilizes the push-push second harmonic oscillator configuration shown in Figure 7, composed of

It is noteworthy that the phase noise of the best commercial state-of-the-art DROs operating in the X and Ku bands typically ranges from -120 down to -150 dBc/Hz at 100-kHz offset (e.g., see the Analog Devices DRO modules and Synergy Microwave DROs). As a good example, the Synergy Microwave 8.32-GHz

DRs with the highest Q-factor are based on sapphire (Al_2O_3) single crystals known for their extremely low dielectric losses [29]. Because of their relatively low ϵ_r , sapphire resonators employ whispering-gallery modes with a high azimuthal index ($n \geq 5$) characterized by low radiation losses that help to reduce the impact of the resonator shielding cavity. These types of resonators are known as whispering-gallery resonators (WGRs) or sapphire loaded cavity (SLC) resonators. At room temperature, the unloaded Q-factor of the SLC resonator can be as high as 200,000 at the X band [29], while at the C-band frequencies it was found to reach 350,000 [32].

To further reduce the phase noise of SLC oscillators, a combined frequency stabilization (CFS) technique is employed. In this technique, the SLC resonator



As follows from the analysis presented in [32], the phase noise floor of the oscillator with CFS is essentially limited by the low-noise amplifier (LNA) noise:

$$S_{\phi}^{\min}(f_m) = S_{\phi}^{\text{LNA}}(f_m) \frac{1}{CS^2} \left\{ 1 + \left(\frac{f_0}{4f_m Q_L} \right)^2 \right\} \quad (21)$$

where CS is the carrier suppression factor: $CS = (1 + \beta_1 + \beta_2)/(1 - \beta_1 + \beta_2)$, and $S_{\phi}^{\text{LNA}}(f_m)$ is the LNA residual phase noise given by

$$S_{\phi}^{\text{LNA}}(f_m) = \left[\frac{k_B T N F C S^2}{P_{\text{in}}^{\text{FD}}} + \frac{b_{-1}}{f_m} \right] \quad (22)$$

where $P_{\text{in}}^{\text{FD}}$ is the power at the FD input, NF is the LNA noise figure, and b_{-1} is the LNA $1/f$ noise. After substituting (22) into (21) and considering that $Q_L \approx Q_0/2$, one gets

$$S_{\phi}^{\min}(f_m) = \left[\frac{k_B T N F}{P_{\text{in}}^{\text{FD}}} + \frac{1}{CS^2} \frac{b_{-1}}{f_m} \right] \left\{ 1 + \left(\frac{f_0}{f_m Q_0} \right)^2 \right\}. \quad (23)$$

The preceding expression is very similar to the minimum phase noise of the feedback oscillator (16) with the exception that the white noise is reduced by a factor of four, while the $1/f$ noise is attenuated by CS^2 . Apart from that, because of the low power level of the signal at the LNA input, the NF in (23) corresponds to the small-signal noise figure, which can be several decibels smaller compared to the large-signal NF used in (16). Thus, in the f^{-2} region, the oscillator with CFS is expected to provide at least 6 dB of phase noise reduction over the optimally designed parallel feedback oscillator. Interestingly, in the case of the $1/f$ noise, the phase noise reduction is considerably higher, given that the carrier suppression factor can be as high as 30–40 dB. This result can be explained by considering very high effective Q-factor of the resonator reflection response, which is essentially proportional to CS and can be significantly higher than Q_0 .

It must be pointed out that, despite their excellent phase noise performance, room-temperature SLC oscillators exhibit a poor short-term frequency stability that suffers from the relatively high frequency–temperature sensitivity of the SLC resonator. Thus, SLC oscillators require a sophisticated temperature stabilization system capable of controlling the resonator temperature with high accuracy [31]. Recently, Ivanov and Tobar [34] have shown that high frequency stability and ultralow phase noise can be simultaneously achieved by locking the SLC oscillator to a highly stable reference. This approach allowed them to achieve a phase noise close to -170 dBc/Hz at an offset frequency of 10 kHz and a fractional frequency instability less than $2 \cdot 10^{-13}$ for integration times from 5 to 50 s.

Another example of ultralow noise microwave oscillators is that of the cryogenically cooled oscillators. The main resonator technology used in this type of oscillator is also SLC resonators, which at the liquid nitrogen temperature (63–77 K) may achieve a Q-factor of $3 \cdot 10^7$. An even higher Q_0 , close to $2 \cdot 10^9$, can be achieved at the liquid helium temperature (4–6 K). Because of these extremely high Q-factors, the cryogenic sapphire oscillators, typically operating around 11 GHz, exhibit a phase noise as low as -96 dBc/Hz at 1-Hz offset and an Allan deviation below 10^{-15} for integration times of 2 to 1,000 s [35]. Such extremely stable oscillators mainly find application in astronomy, fundamental physics, and quantum information experiments [36].

Chaudy et al. [37] recently reported a novel low-noise cryogenic 1-GHz oscillator based on a planar high-temperature superconducting resonator. The proposed oscillator operates at 65 K, has a much smaller form factor when compared to the cryogenic sapphire oscillators, and exhibits a phase noise of -137 dBc/Hz at 1-kHz offset, which is comparable to the best commercial oven-controlled crystal and SAW oscillators. The phase noise floor of the reported oscillator is close to -170 dBc/Hz and is limited by the resonator input power.

Notably, because of Q-factor degradation with frequency, the phase noise performance of oscillators based on conventional resonators worsens considerably when the operating frequency extends into the millimeter-wave bands. To overcome this issue, recently, several novel high-frequency resonant structures have been developed allowing one to considerably improve the phase noise of millimeter-wave oscillators. Lia et al. [38] have reported an ultralow-noise millimeter-wave oscillator based on a novel electromagnetic bandgap (EBG) resonator using a periodic structure implemented on an ultrahigh resistivity silicon wafer. Utilizing this approach, the authors were able to achieve a phase noise of -142 dBc/Hz at 100-kHz offset, which was mainly possible because of the very high Q-factor (108,500 at 45.8 GHz) of the EBG resonator. Another millimeter-wave oscillator operating above 30 GHz with a remarkably low phase noise of -149 dBc/Hz at 100-kHz offset was reported by Poddar et al. [39]. In their design, the authors used a novel split-ring resonator structure exhibiting an unloaded Q-factor of 11,658 at 30.2 GHz.

Voltage-Controlled Oscillators

Voltage-controlled oscillators (VCOs) are the most widely used type of oscillator employed in wireless communication systems and other microwave and RF applications requiring a tunable frequency source. Standalone VCOs are frequently implemented using MMIC technology, or they can be a part of a larger chip that may contain multiple RF blocks.

Currently, there are a number of semiconductor technologies available for integrated VCO implementation. CMOS VCOs can be considered one of the most studied oscillators because of the broad adoption of CMOS technology. One frequently used CMOS VCO topology is the cross-coupled oscillator shown in Figure 9. This fairly simple configuration uses a pair of identical MOS transistors having a balanced parallel LC tank as a load [40]. It can be considered by far the most popular VCO configuration because of its low phase noise, high power efficiency, and balanced output.

The phase noise of the cross-coupled VCO is given by

$$\mathcal{L}(f_m) = \left[\frac{k_B T F R_p}{2V_p^2} \left(\frac{f_0}{f_m Q_t} \right)^2 \right] \quad (24)$$

where Q_t is the equivalent Q-factor of the LC tank, and V_p is the maximum oscillation voltage amplitude, R_p is the tank impedance magnitude, and F is the effective noise factor of the oscillator. Along with the phase noise, the VCO FoM introduced earlier (17) is also considered an important specification, and it can be expressed as follows [45]:

$$\text{FoM}(f_m) = -10 \log \left(\frac{10^3 k_B T F}{2Q_t^2 \alpha_V \alpha_I} \right) \quad (25)$$

where $\alpha_I = i_{d1}/I_B$ is the current conversion efficiency of the oscillator, and $\alpha_V = V_p/V_{DD}$ is the voltage efficiency. The effective noise factor F includes noise contributions from the LC tank, the MOS transistor channel conductance, and the MOS transconductance. The noise factor calculation involves the VCO impulse sensitivity

function, which is a key parameter in the linear time-varying phase noise model. Using expression (25), one can estimate that for a conventional class-B VCO with $Q_t = 15$, $\alpha_I = 0.55$, $\alpha_V = 0.8$, and $F = 5.5$ dB [45], the expected FoM is 191.3 dBc/Hz. In practice, a VCO FoM of 190 dBc/Hz or higher is considered a very good result.

To improve both the VCO phase noise and FoM, a number of different oscillator classes have been proposed. Table 2 presents a performance comparison for the VCOs with the best reported FoMs based on different oscillator approaches [41], [42], [43], [44], [45],

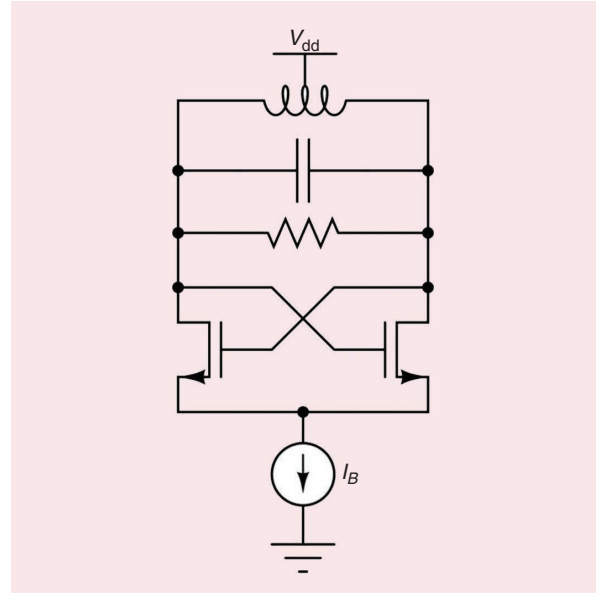


Figure 9. CMOS cross-coupled oscillator.

TABLE 2. Comparative performance of CMOS VCOs.

Ref.	VCO Topology	Tuning Range, GHz	DC Power, mW	Tank Q-Factor	FOM @ 1 MHz, dBc/Hz	PN @ 1 MHz, dBc/Hz
[41]	350-nm CMOS cross-coupled VCO	2.15–2.35	10	11	192.2	–135
[42]	55-nm CMOS Class B	7.35–8.4	6.3	15	190.4	–121
[43]	130-nm CMOS Class C	4.9–5.65	1.4	16–17	194.8	–122.5
[44]	65-nm CMOS Class D	3–4.8	8.5	14	190.2	–130 ¹
[45]	65-nm CMOS Class F	5.9–7.6	15	16	190.6	–125 ²
[46]	65-nm CMOS Class F ₂	5–6.36	6.1	14.3/19.5*	194.5	–128.4 ³
[47]	65-nm CMOS Class F ₂₃	18.5–22.4	5	21**	189	–110.7
[48]	65-nm CMOS Class F ^{–1}	3.49–4.51	1.2	14	195.2	–125.1 ⁴
[49]	22-nm FDSOI folded DCO	4.15–4.97	1.22	11–17	194.7	–120 ⁵
[50]	130-nm CMOS QVCO	23.65–24.85	3.86	20.4/22*	201.1	–119.4
[51]	130-nm CMOS Dual Tank	4.8–5.34	74	17.4	192.4	–137 ⁶

¹ $F_{VCO} = 3$ GHz, $V_{dd} = 0.5$ V.

² $F_{VCO} = 7.4$ GHz.

³ $F_{VCO} = 5$ GHz, $V_{dd} = 0.4$ V.

⁴ $F_{VCO} = 3.49$ GHz, $V_{dd} = 0.6$ V.

⁵ $F_{VCO} = 4.97$ GHz, $V_{dd} = 0.15$ V.

⁶ $F_{VCO} = 5.08$ GHz, $V_{dd} = 0.85$ V.

*Simulated transformer Q-factor (Q_p/Q_s).

**Simulated inductor Q-factor.

FD-SOI: fully depleted silicon-on-insulator; QVCO: quadrature voltage-controlled oscillator.

[46], [47], [48], [49], [50], [51]. As one may notice, most of the reported VCOs exhibit FoMs > 190 dBc/Hz. The highest FoMs have been achieved in the VCOs using class-C [43], class- F_2 [46], and class- F^{-1} [48] oscillator approaches. In particular, an excellent FoM has been reported for the Class- F^{-1} VCO, shown in Figure 10. It employs a transformer-based LC tank, providing high-Q resonances at the first and second harmonics that help to reduce the transistor noise upconversion by properly shaping the drain voltage waveform [48]. Another CMOS VCO with a remarkably high FoM of 201.1 dBc/Hz at 1-MHz offset was reported by Jalalifar and Byun [50]. Their design is based on a quadrature VCO topology that contains two coupled differential oscillator cores and uses an innovative high-Q transformer-based feedback network.

It is worth mentioning that for VCOs with a large FTR, the phase noise can be strongly impacted by the varactor frequency tuning network. In this case, phase noise degradation is caused by both reduction of the LC-tank Q-factor impacted by the varactor losses and also the nonlinearity of the varactor $C(V)$ response causing AM-to-PM conversion, which becomes more pronounced when the varactors are biased close to 0 V. The AM-to-PM conversion can be minimized, for example, by using a back-to-back varactor configuration.

In the case of integrated VCOs, to achieve a wide FTR and preserve low phase noise, a combination of coarse and fine tuning is used. For coarse tuning, a high-Q digitally switched capacitor array with metal-insulator-metal or metal-oxide-metal (MOM) capacitors is typically employed. The varactors are utilized to provide fine, continuous tuning. Thus, in the previous described Class- F^{-1} VCO, the C_p and C_s employ 6-bit and 5-bit MOM switchable capacitors, and additional MOS varactors provide fine tuning.

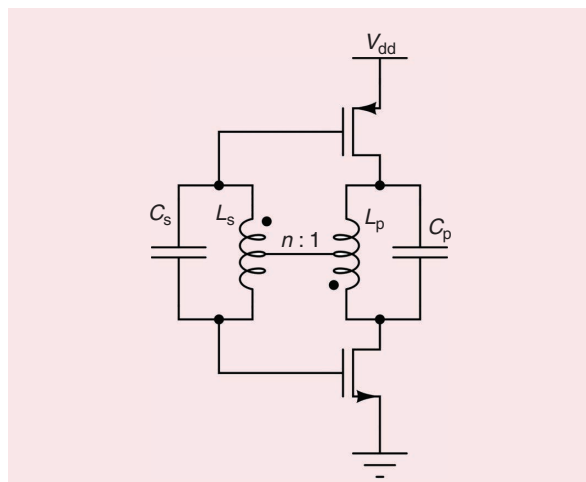


Figure 10. Inverse Class-F CMOS VCO.

We note that the FTR can also be increased without sacrificing the phase noise or FoM by using multicore coupled oscillators with mode switching. Recently, El-Aassar and Rebeiz [52] reported a transformer-based dual-core switched-mode VCO with octave tuning that achieved a 191-dBc/Hz FoM. Interestingly, Wu et al. recently also reported a switchless dual-core triple-mode VCO intended for a quantum bit control application that covers a 7.1–15.7-GHz frequency range and achieves a peak FoM of 202.1 dBc/Hz at 10-MHz offset while operating at a temperature of 3.7 K [53]. In this design, mode switching is implemented by enabling/disabling different negative transconductance VCO cells rather than using lossy MOS switches, thus improving the overall VCO performance.

As demonstrated, CMOS VCOs, because of their low supply voltage and high dc-to-RF conversion efficiency, offer excellent performance in terms of FoM. However, they exhibit relatively high $1/f$ noise ($f_c = 0.1$ –1 MHz) as well as a low Q-factor that typically does not exceed 15–20 [54]. As mentioned earlier, microwave oscillators based on HBTs exhibit the lowest phase noise because of the inherently low $1/f$ noise of the bipolar devices. Currently, these types of oscillators are commonly implemented using SiGe BiCMOS, GaAs, and InP HBT technologies. In particular, the InP-based HBT technology, with its high transition frequency ($f_t = 300$ –600 GHz) and high breakdown voltage, is especially attractive for microwave and millimeter-wave VCOs up to several hundreds of gigahertz. The best phase noise results reported for integrated HBT-based VCOs [55], [56], [57], [58], [59], [60], [61], [62], [63], [64], [65] as well as for some commercially available MMIC VCOs (MACOM InGaP HBT-based VCOs) are presented in Figure 11. As one may observe, below 10 GHz the HBT-based VCOs exhibit a phase noise lower than -130 dBc/Hz at 1-MHz offset. As expected, the VCO phase noise increases with frequency, reaching approximately -85 dBc/Hz in the 300-GHz band. Interestingly, some VCO designs, shown in Figure 11 with diamonds, achieve an 8–10-dB lower phase noise when compared to the general trend. Thus, Franceschin et al. reported an ultralow phase noise X-band BiCMOS VCO based on a series LC tank achieving a phase noise of -138 dBc/Hz at 1-MHz offset [64]. As reported, this improvement was possible because of the considerably higher RF power dissipated in the series LC tank when compared to the commonly used parallel tanks. Another ultralow noise 20-GHz VCO reported by Riccardi et al. [65] is based on the large oscillator array approach, which allowed them to reduce the phase noise by $10\log(N)$, where N is the number of independent oscillator cores. The proposed design employs 16 VCO cores and achieves a remarkable phase noise of -128 dBc/Hz at 1-MHz offset.

It is important to note that some of the commercially available narrow-band VCOs operating in the 5–12-GHz frequency range also exhibit excellent phase noise values that are lower than –135 dBc/Hz at 1-MHz offset (e.g., MACOM MAOC-009262/009871 and the Analog Devices HMC-116x family). The FTR of this type of VCO is typically about 20%, and the FoM is close to 190 dBc/Hz.

In some applications, typically below 10 GHz, the VCOs can also be implemented using tunable resonators or filters based on planar technologies, like microstrips or coplanar waveguides. In contrast to the LC tanks used in the integrated VCOs, this type of resonator offers a significantly higher Q-factor; hence, microstrip-based VCOs typically exhibit better phase noise performance. Rohde and Poddar reported ultralow noise 1–4-GHz VCOs based on tunable coupled microstrip resonators with phase noise values better than –114 dBc/Hz and –134 dBc/Hz at 100-kHz and 1-MHz offsets, respectively [66]. The authors also reported miniaturized 4–8-GHz and 8–12-GHz VCOs achieving phase noise values of –130 dBc/Hz and –125 dBc/Hz at 1-MHz offset. These results are comparable to those of the best state-of-the-art integrated oscillators; however, because of the innovative design, the proposed microstrip-based VCOs offer a much wider tuning range.

Yttrium Iron Garnet Tuned Oscillators

The yttrium iron garnet (YIG) tuned oscillators (YTOs) are microwave oscillators with broadband electronic frequency tuning and excellent phase noise performance. They are mainly used in test and measurement equipment requiring a tunable high-performance frequency source. This type of oscillator employs YIG resonators that rely on spin precession resonance occurring in the ferromagnetic materials, and their frequency is linearly proportional to the magnitude of the applied external magnetic field H_0 :

$$f_0 = \gamma H_0 \quad (26)$$

where $\gamma = g\mu_B/\hbar$ is a constant known as the *gyromagnetic ratio* and is equal to 2.8 MHz/Oe, g is the Landé factor, μ_B is the Bohr magneton, and \hbar is the reduced Planck's constant.

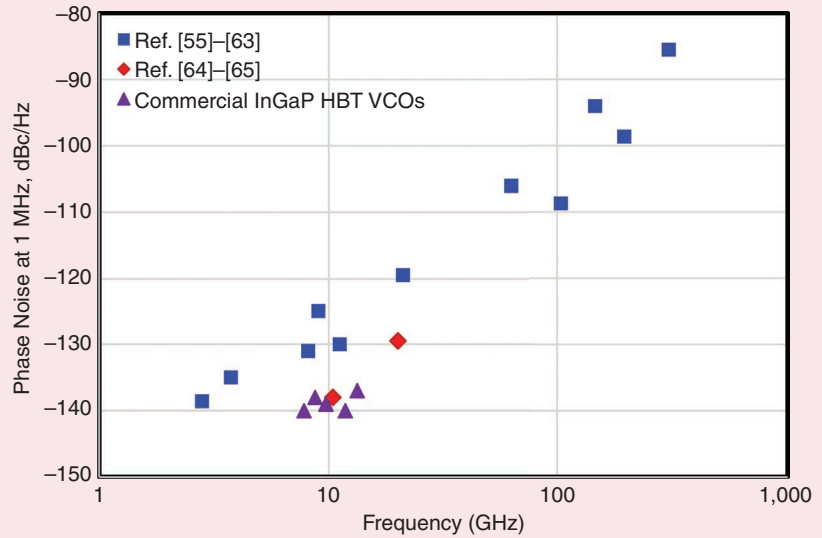


Figure 11. Phase noise of integrated HBT-based VCOs.

Also, the Q-factor of the YIG is governed by the resonance linewidth:

$$Q_0 = \frac{\frac{f_0}{\gamma} - \frac{1}{3}4\pi M_s}{\Delta H} \quad (27)$$

where ΔH is the resonance linewidth in oersteds, and the quantity $4\pi M_s$ is the saturation magnetization in gauss, which for a pure YIG sphere equals 1,780 G. Because of the very small linewidth with typical values of $\Delta H = 0.4$ – 0.5 Oe, Q_0 of the YIG resonator can be as high as 6,000. Interestingly, for YIG, Q_0 is linearly dependent on the resonance frequency, which is not typical for the other types of high-Q microwave resonators, which have constant Qf ; i.e., their Q decreases linearly with frequency. Most YTOs utilize spherical YIG resonators of small diameter (typically 10–20 mm) with an attached BeO ceramic rod used as a support. Depending on the YTO configuration, the YIG sphere may have one or two coupling loops with a diameter about two times larger than that of the sphere.

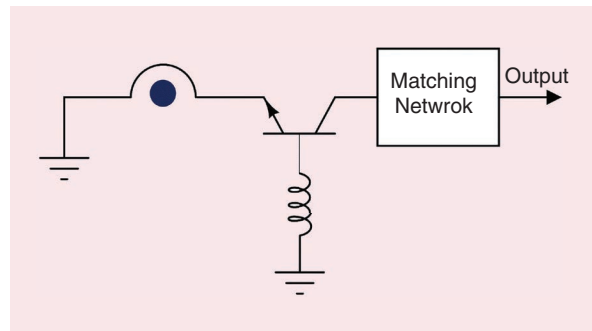


Figure 12. Simplified YTO schematic.

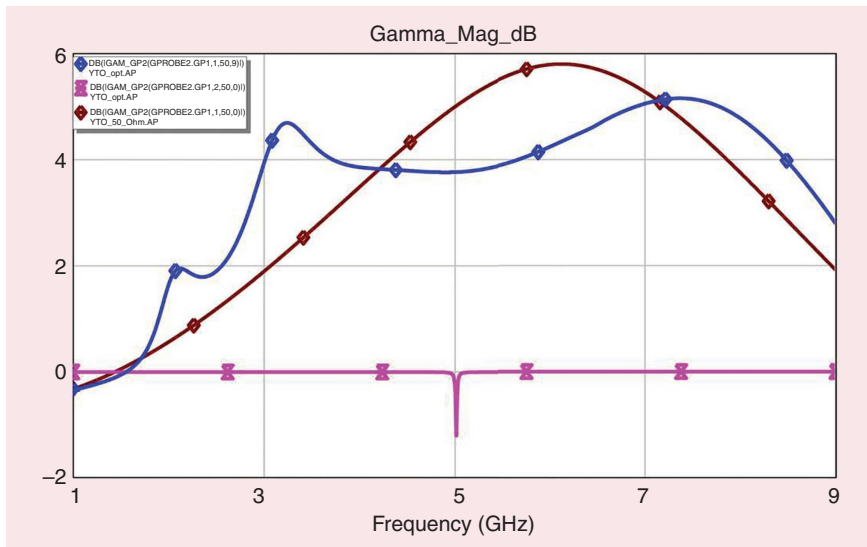


Figure 13. Responses of the active device and YIG resonator reflection coefficients.

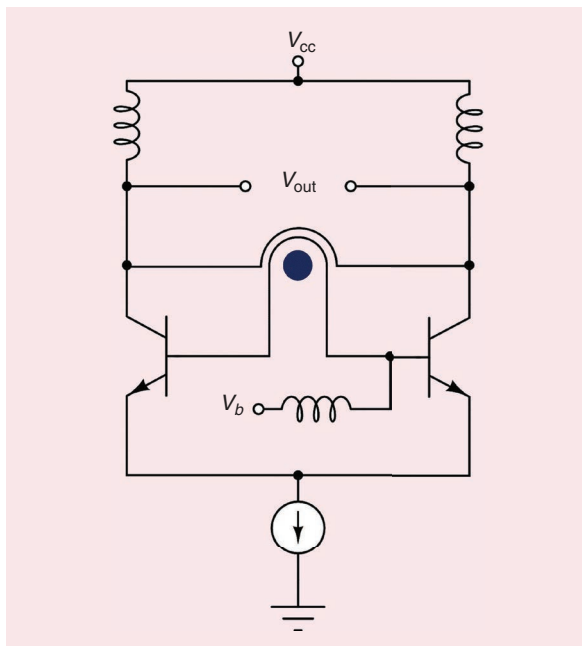


Figure 14. Differential MMIC-based YTO.

Typically, YTOs operate at frequencies between 1 and 40 GHz, providing FTR values of 65%–85%. Some YTO designs using composite feedback may achieve an FTR as wide as 160% [67]. As mentioned, state-of-the-art YTOs exhibit excellent phase noise values that range from -125 to -133 dBc/Hz at 100-kHz offset [68]. In contrast to the other types of oscillators, the YTO phase noise has no pronounced dependence on the oscillation frequency because of the aforementioned YIG Q-factor increase with frequency. A simplified schematic that is widely used for YTO implementation is shown in Figure 12. Essentially, it contains a discrete active

device (e.g., a BJT, a GaAs field-effect transistor, etc.), which provides negative resistance in the wide frequency range, and a YIG sphere coupled to the active device using a small magnetic loop. For the YTO design, a negative resistance oscillator model is commonly used. As an example, Figure 13 presents the reflection coefficient responses of the active device and YIG resonator calculated using a commercial CAD software. In this particular case, the active device response is optimized to cover a 2–9-GHz frequency range by providing proper impedance at the active device output.

An innovative differential YTO utilizing a ring oscillator topology with a YIG filter was proposed by Sweet and Parrott [69]. As shown in Figure 14, this YTO employs an MMIC-based differential amplifier coupled to the YIG sphere using two coupling loops. Because of the use of a dedicated MMIC with flat broadband gain response, the oscillator does not require the manual tuning that is commonly needed in YTOs based on discrete active devices. A similar differential oscillator approach has been used by van Delden et al. for 19.1–41.4-GHz and 32–48.2-GHz YTOs [70]. The proposed oscillators use a low-noise MMIC amplifier based on 130-nm SiGe:C BiCMOS technology, and they exhibit excellent phase noise values lower than -120 dBc/Hz at 100-kHz offset for oscillation frequencies up to 38 GHz.

We note that state-of-the-art commercial YTOs cover frequencies from 0.7 to 40 GHz. They typically exhibit phase noise values better than -120 dBc/Hz at 100-kHz offset and may provide frequency tuning of up to 160% (e.g., the Teledyne FS2722 and Micro Lambda Wireless MLXS-T series). Furthermore, Teledyne permanent-magnet-based ultralow noise TINYig YTOs offer the same outstanding phase noise performance and have one of the smallest form factors in the industry.

Conclusion

In the past 20 years, driven by the wireless industry and other related technology fields, the performance of microwave oscillators has seen significant improvements that were made possible by the impressive advances in both semiconductor and resonator technologies. The development of more accurate oscillator models and advanced phase noise reduction techniques has also played a crucial role in the improvement of

oscillator spectral purity, which continues to remain one of the key requirements constantly challenged by industry demands as well as by emerging technologies and novel applications.

References

- [1] K. Kurokawa, "Some basic characteristics of broadband negative resistance oscillator circuits," *Bell Syst. Tech. J.*, vol. 48, no. 6, pp. 1937–1955, Jul. 1969, doi: [10.1002/j.1538-7305.1969.tb01158.x](#).
- [2] P. Roblin, *Nonlinear RF Circuits and Nonlinear Vector Network Analyzers: Interactive Measurement and Design Techniques*. Cambridge, U.K.: Cambridge Univ. Press, 2011.
- [3] S. A. Maas, *Noise in Linear and Nonlinear Circuits*. Norwood, MA, USA: Artech House, 2005.
- [4] D. B. Leeson, "A simple model of feedback oscillator noise spectrum," *Proc. IEEE*, vol. 54, no. 2, pp. 329–330, Feb. 1966, doi: [10.1109/PROC.1966.4682](#).
- [5] R. Boudot and E. Rubiola, "Phase noise in RF and microwave amplifiers," *IEEE Trans. Ultrason., Ferroelectr., Freq. Control*, vol. 59, no. 12, pp. 2613–2624, Dec. 2012, doi: [10.1109/TUFFC.2012.2502](#).
- [6] M. Jankovic, J. Breitbarth, A. Brannon, and Z. Popovic, "Measuring transistor large-signal noise figure for low-power and low phase-noise oscillator design," *IEEE Trans. Microw. Theory Techn.*, vol. 56, no. 7, pp. 1511–1515, Jul. 2008, doi: [10.1109/TMTT.2008.924350](#).
- [7] A. Hati, D. A. Howe, F. L. Walls, and D. Walker, "Noise figure vs. PM noise measurements: A study at microwave frequencies," in *Proc. IEEE Int. Freq. Control Symp. Joint 17th Eur. Freq. Time Forum*, 2003, pp. 516–520, doi: [10.1109/FREQ.2003.1275144](#).
- [8] E. Rubiola, *Phase Noise and Frequency Stability in Oscillators*. Cambridge, U.K.: Cambridge Univ. Press, 2009.
- [9] M. A. Margarit, J. Leong Tham, R. G. Meyer, and M. J. Deen, "A low-noise, low-power VCO with automatic amplitude control for wireless applications," *IEEE J. Solid-State Circuits*, vol. 34, no. 6, pp. 761–771, Jun. 1999, doi: [10.1109/4.766810](#).
- [10] T. N. T. Do, M. Hörberg, S. Lai, and D. Kuylenstierna, "Low frequency noise measurements - A technology benchmark with target on oscillator applications," in *Proc. 44th Eur. Microw. Conf.*, 2014, pp. 1412–1415, doi: [10.1109/EuMC.2014.6986710](#).
- [11] T. Felgentreff, W. Anzill, G. Olbrich, and P. Russer, "Analysis of g-r noise upconversion in oscillators," in *Proc. IEEE MTT-S Int. Microw. Symp.*, 1995, vol. 2, pp. 947–950, doi: [10.1109/MWSYM.1995.405892](#).
- [12] I. D. Avramov, "Characterization of single-port surface transverse wave resonators in the lower GHz range," in *Proc. Joint Eur. Freq. Time Forum IEEE Int. Freq. Control Symp.*, 1999, vol. 2, pp. 863–866, doi: [10.1109/FREQ.1999.841441](#).
- [13] P. Dufilie, J. V. Adler, and A. Sawyer, "Performances of monolithic micro-oven heated SAW and STW resonators," in *Proc. IEEE Int. Ultrason. Symp.*, 2011, pp. 87–91, doi: [10.1109/ULTSYM.2011.0022](#).
- [14] J.-H. Lin and Y.-H. Kao, "A low phase-noise voltage-controlled SAW oscillator with surface transverse wave resonator for SONET application," *IEEE Trans. Microw. Theory Techn.*, vol. 55, no. 1, pp. 60–65, Jan. 2007, doi: [10.1109/TMTT.2006.888575](#).
- [15] M. Ueda et al., "High-Q resonators using FBAR/SAW technology and their applications," in *Proc. IEEE MTT-S Int. Microw. Symp.*, 2005, pp. 209–212, doi: [10.1109/MWSYM.2005.1516561](#).
- [16] A. Nelson, J. Hu, J. Kaitila, R. Ruby, and B. Otis, "A 22 μ W, 2.0 GHz FBAR oscillator," in *Proc. IEEE Radio Freq. Integr. Circuits Symp.*, 2011, pp. 1–4, doi: [10.1109/RFIC.2011.5940708](#).
- [17] R. Parker et al., "Effects of FBAR resonator dissipated power on discrete oscillator phase noise," in *Proc. IEEE Int. Ultrason. Symp.*, 2014, pp. 93–96, doi: [10.1109/ULTSYM.2014.0024](#).
- [18] A. Imani and H. Hashemi, "A low-noise FBAR-CMOS frequency/phase discriminator for phase noise measurement and cancellation," in *Proc. IEEE Radio Freq. Integr. Circuits Symp.*, 2013, pp. 431–434, doi: [10.1109/RFIC.2013.6569623](#).
- [19] D. Gachon, E. Courjon, J. Masson, V. Petrini, J. Y. Rauch, and S. Balandras, "PIH-1 LiNbO_3 - LiNbO_3 high overtone bulk acoustic resonator exhibiting high Q \cdot f product," in *Proc. IEEE Ultrason. Symp.*, 2007, pp. 1417–1420, doi: [10.1109/ULTSYM.2007.356](#).
- [20] R. Boudot, G. Martin, J.-M. Friedt, and E. Rubiola, "Frequency flicker of 2.3 GHz AlN -Sapphire high-overtone bulk acoustic resonators," *J. Appl. Phys.*, vol. 120, no. 22, 2016, Art. no. 224903, doi: [10.1063/1.4972102](#).
- [21] H. Yu et al., "HBAR-Based 3.6 GHz oscillator with low power consumption and low phase noise," *IEEE Trans. Ultrason., Ferroelectr., Freq. Control*, vol. 56, no. 2, pp. 400–403, Feb. 2009, doi: [10.1109/TUFFC.2009.1050](#).
- [22] U. L. Rohde, "Ceramic resonator oscillators challenge SAW performance," *Microw. RF*, vol. 42, no. 9, pp. 100–105, 2003.
- [23] M. T. Sebastian, *Dielectric Materials for Wireless Communication*. Amsterdam, The Netherlands, Elsevier, 2010.
- [24] J. Everard and K. Theodoropoulos, "Ultra-low phase noise ceramic based dielectric resonator oscillators," in *Proc. IEEE Int. Freq. Control Symp.*, 2006, pp. 869–874, doi: [10.1109/FREQ.2006.275503](#).
- [25] P. D. Deshpande and J. Everard, "Compact low phase noise 3.8 GHz oscillator," in *Proc. Eur. Freq. Time Forum*, 2014, pp. 203–207, doi: [10.1109/EFTF.2014.7331466](#).
- [26] M. Sallin, L. Zhou, C. Broomfield, and J. Everard, "Broad tuning ultra-low noise DROs at 10 GHz utilizing ceramic based resonators," in *Proc. IEEE Int. Freq. Control Symp. Joint 17th Eur. Freq. Time Forum*, 2003, pp. 411–416, doi: [10.1109/FREQ.2003.1275127](#).
- [27] C. Florian, P. A. Traverso, G. Vannini, and F. Filicori, "Design of low phase noise dielectric resonator oscillators with GaInP HBT devices exploiting a non-linear noise model," in *Proc. IEEE MTT-S Int. Microw. Symp.*, 2007, pp. 1525–1528, doi: [10.1109/MWSYM.2007.380563](#).
- [28] Q. Xia, Z. Tang, and B. Zhang, "Design of a 17.4GHz push-push dielectric resonator oscillator," in *Proc. Int. Conf. Microw. Millimeter-Wave Techn.*, Chengdu, China, 2010, pp. 532–535, doi: [10.1109/ICMMT.2010.5525221](#).
- [29] J. G. Hartnett, M. E. Tobar, E. N. Ivanov, and J. Krupka, "Room temperature measurement of the anisotropic loss tangent of sapphire using the whispering gallery mode technique," *IEEE Trans. Ultrason., Ferroelectr., Freq. Control*, vol. 53, no. 1, pp. 34–38, Jan. 2006, doi: [10.1109/TUFFC.2006.1588389](#).
- [30] G. Cibiel et al., "Optimization of an ultra low-phase noise sapphire-SiGe HBT oscillator using nonlinear CAD," *IEEE Trans. Ultrason., Ferroelectr., Freq. Control*, vol. 51, no. 1, pp. 33–41, Jan. 2004, doi: [10.1109/TUFFC.2004.1268465](#).
- [31] R. Boudot et al., "Development of ultra low phase noise X-band oscillators," in *Proc. IEEE Int. Freq. Control Symp. Expo.*, 2006, pp. 861–868, doi: [10.1109/FREQ.2006.275502](#).
- [32] N. Shitn and J. M. L. Romero, "Ultra low phase noise C-band oscillators with combined frequency stabilization," in *Proc. Asia-Pacific Microw. Conf.*, Yokohama, Japan, 2010, pp. 378–381.
- [33] E. N. Ivanov and M. E. Tobar, "Low phase-noise sapphire crystal microwave oscillators: Current status," *IEEE Trans. Ultrason., Ferroelectr., Freq. Control*, vol. 56, no. 2, pp. 263–269, Feb. 2009, doi: [10.1109/TUFFC.2009.1035](#).
- [34] E. N. Ivanov and M. E. Tobar, "Frequency stable microwave sapphire oscillators," *IEEE Microw. Wireless Technol. Lett.*, vol. 33, no. 12, pp. 1642–1645, Dec. 2023, doi: [10.1109/LMWT.2023.3318530](#).
- [35] J. G. Hartnett, N. R. Nand, C. Wang, and J.-m. L. Floch, "Cryogenic sapphire oscillator using a low-vibration design pulse-tube cryocooler: First results," *IEEE Trans. Ultrason., Ferroelectr., Freq. Control*, vol. 57, no. 5, pp. 1034–1038, May 2010, doi: [10.1109/TUFFC.2010.1515](#).
- [36] T. R. Tan et al., "Improving a trapped-ion quantum computer with a cryogenic sapphire oscillator," in *Proc. Joint Conf. Eur. Freq. Time Forum IEEE Int. Freq. Control Symp. (EFTF/IFCS)*, 2023, pp. 1–2, doi: [10.1109/EFTF/IFCS57587.2023.10272197](#).
- [37] D. Chaudy et al., "A low phase noise all cryogenic microwave oscillator based on a superconductor resonator," *IEEE Trans. Ultrason., Ferroelectr., Freq. Control*, vol. 67, no. 12, pp. 2750–2756, Dec. 2020, doi: [10.1109/TUFFC.2020.3023198](#).
- [38] E. Lia et al., "Novel mm-Wave oscillator based on an electromagnetic bandgap resonator," *IEEE Microw. Wireless Technol. Lett.*, vol. 33, no. 6, pp. 863–866, Jun. 2023, doi: [10.1109/LMWT.2023.3268090](#).

- [39] A. K. Poddar, U. L. Rohde, V. Madhavan, A. M. Apte, and S. K. Koul, "Ka-band metamaterial Möbius Oscillator (MMO) circuit," in *Proc. IEEE MTT-S Int. Microw. Symp.*, 2016, pp. 1–4, doi: [10.1109/MWSYM.2016.7539970](#).
- [40] J. Craninckx and M. Steyaert, "A CMOS 1.8 GHz low-phase-noise voltage-controlled oscillator with prescaler," in *Proc. Int. Solid-State Circuits Conf.*, 1995, pp. 266–267, doi: [10.1109/ISSCC.1995.535550](#).
- [41] P. Andreani and A. Fard, "More on the $1/f^2$ phase noise performance of CMOS differential-pair LC-tank oscillators," *IEEE J. Solid-State Circuits*, vol. 41, no. 12, pp. 2703–2712, Dec. 2006, doi: [10.1109/JSSC.2006.884188](#).
- [42] M. Garampazzi, P. M. Mendes, N. Codega, D. Manstretta, and R. Castello, "Analysis and design of a 195.6 dBc/Hz peak FoM P-N class-B oscillator with transformer-based tail filtering," *IEEE J. Solid-State Circuits*, vol. 50, no. 7, pp. 1657–1668, Jul. 2015, doi: [10.1109/JSSC.2015.2413851](#).
- [43] A. Mazzanti and P. Andreani, "Class-C harmonic CMOS VCOs, with a general result on phase noise," *IEEE J. Solid-State Circuits*, vol. 43, no. 12, pp. 2716–2729, Dec. 2008, doi: [10.1109/JSSC.2008.2004867](#).
- [44] L. Fanori and P. Andreani, "Class-D CMOS oscillators," *IEEE J. Solid-State Circuits*, vol. 48, no. 12, pp. 3105–3119, Dec. 2013, doi: [10.1109/JSSC.2013.2271531](#).
- [45] M. Babaie and R. B. Staszewski, "A class-F CMOS oscillator," *IEEE J. Solid-State Circuits*, vol. 48, no. 12, pp. 3120–3133, Dec. 2013, doi: [10.1109/JSSC.2013.2273823](#).
- [46] H. Guo, Y. Chen, P.-I. Mak, and R. P. Martins, "20.1 A 5.0-to-6.36 GHz wideband-harmonic-shaping VCO achieving 196.9 dBc/Hz Peak FoM and 90-to-180 kHz $1/f^3$ PN corner without harmonic tuning," in *Proc. IEEE Int. Solid-State Circuits Conf.*, 2021, pp. 294–296, doi: [10.1109/ISSCC42613.2021.9365761](#).
- [47] S. Tian and X. Liu, "A 18.5-to-22.4 GHz class-F23 VCO achieving 189.1 dBc/Hz FoM without 2nd/3rd harmonic tuning in 65 nm CMOS," in *Proc. IEEE 49th Eur. Solid-State Circuits Conf.*, 2023, pp. 129–132, doi: [10.1109/ESSCIRC59616.2023.10268771](#).
- [48] C. C. Lim, H. Ramiah, J. Yin, P.-I. Mak, and R. P. Martins, "An inverse-class-F CMOS oscillator with intrinsic-high-Q first harmonic and second harmonic resonances," *IEEE J. Solid-State Circuits*, vol. 53, no. 12, pp. 3528–3539, Dec. 2018, doi: [10.1109/JSSC.2018.2875099](#).
- [49] O. El-Aassar and G. M. Rebeiz, "26.5 A 0.1-to-0.2 V transformer-based switched-mode folded DCO in 22 nm FDSOI with active step-down impedance achieving 197 dBc/Hz Peak FoM and 40 MHz/V frequency pushing," in *Proc. IEEE Int. Solid-State Circuits Conf.*, 2019, pp. 416–418, doi: [10.1109/ISSCC.2019.8662516](#).
- [50] M. Jalalifar and G.-S. Byun, "A current-reused back-gate coupling QVCO using transformer feedback structure," *IEEE Microw. Wireless Compon. Lett.*, vol. 26, no. 7, pp. 534–536, Jul. 2016, doi: [10.1109/LMWC.2016.2575018](#).
- [51] F. L. Pour, D. S. Ha, and A. Nikpaik, "An ultra-low phase noise dual-tank oscillator featuring tank impedance scaling," *IEEE Trans. Circuits Syst. I, Reg. Papers*, vol. 71, no. 12, pp. 5657–5668, Dec. 2024, doi: [10.1109/TCSI.2024.3443752](#).
- [52] O. El-Aassar and G. M. Rebeiz, "Octave-tuning dual-core folded VCO leveraging a triple-mode switch-less tertiary magnetic loop," *IEEE J. Solid-State Circuits*, vol. 56, no. 5, pp. 1475–1486, May 2021, doi: [10.1109/JSSC.2021.3059442](#).
- [53] Y. Wu, Y. Peng, B. Huo, J. Yin, R. P. Martins, and P. I. Mak, "A switchless dual-core triple-mode VCO achieving 7.1-to-15.7 GHz frequency tuning range and 202.1 dBc/Hz Peak FoM at 3.7 Kelvin," in *Proc. IEEE Radio Freq. Integr. Circuits Symp.*, 2024, pp. 243–246, doi: [10.1109/RFIC61187.2024.10600042](#).
- [54] J. R. Long, Y. Zhao, W. Wu, M. Spirito, L. Vera, and E. Gordon, "Passive circuit technologies for mm-Wave wireless systems on silicon," *IEEE Trans. Circuits Syst. I, Reg. Papers*, vol. 59, no. 8, pp. 1680–1693, Aug. 2012, doi: [10.1109/TCSI.2012.2206499](#).
- [55] F. Boscolo, F. Padovan, F. Quadrelli, M. Tiebout, A. Neviani, and A. Bevilacqua, "A 21 GHz 20.5%-tuning range Colpitts VCO with -119 dBc/Hz phase noise at 1 MHz offset," in *Proc. 43rd IEEE Eur. Solid-State Circuits Conf.*, 2017, pp. 91–94, doi: [10.1109/ESSCIRC.2017.8094533](#).
- [56] Y. Sun and C. J. Scheytt, "A low-phase-noise 61 GHz push-push VCO with divider chain and buffer in SiGe BiCMOS for 122 GHz ISM applications," in *Proc. IEEE Radio Freq. Integr. Circuits Symp.*, 2012, pp. 79–82, doi: [10.1109/RFIC.2012.6242236](#).
- [57] M. Hossain, N. Weimann, W. Heinrich, and V. Krozer, "Highly efficient D-band fundamental frequency source based on InP-DHBT technology," in *Proc. 48th Eur. Microw. Conf.*, 2018, pp. 1005–1008, doi: [10.23919/EuMC.2018.8541599](#).
- [58] H. Khatibi, S. Khiyabani, A. Cathelin, and E. Afshari, "A 195 GHz single-transistor fundamental VCO with 15.3% DC-to-RF efficiency, 4.5 mW output power, phase noise FoM of -197 dBc/Hz and 1.1% tuning range in a 55 nm SiGe process," in *Proc. IEEE Radio Freq. Integr. Circuits Symp.*, 2017, pp. 152–155, doi: [10.1109/RFIC.2017.7969040](#).
- [59] D. Kuylenstierna, S. Lai, M. Bao, and H. Zirath, "Design of low phase-noise oscillators and wideband VCOs in InGaP HBT technology," *IEEE Trans. Microw. Theory Techn.*, vol. 60, no. 11, pp. 3420–3430, Nov. 2012, doi: [10.1109/TMTT.2012.2216893](#).
- [60] X. Cheng, F.-J. Chen, X.-L. Xia, J.-A. Han, X.-H. Luo, and Z.-C. Zhao, "A modified Darlington-based class-C VCO with simultaneous optimization of phase noise/FoM in GaAs technology," *IEEE Microw. Wireless Compon. Lett.*, vol. 30, no. 5, pp. 500–503, May 2020, doi: [10.1109/LMWC.2020.2983845](#).
- [61] C. Florian, S. D'Angelo, D. Resca, and F. Scappaviva, "A chip set of low phase noise MMIC VCOs at C, X and Ku band in InGaP-GaAs HBT technology for satellite telecommunications," in *Proc. IEEE MTT-S Int. Microw. Symp.*, 2017, pp. 1148–1151, doi: [10.1109/MWSYM.2017.8058802](#).
- [62] J. Yun, D. Yoon, H. Kim, and J.-S. Rieh, "300-GHz InP HBT oscillators based on common-base cross-coupled topology," *IEEE Trans. Microw. Theory Techn.*, vol. 62, no. 12, pp. 3053–3064, Dec. 2014, doi: [10.1109/TMTT.2014.2364608](#).
- [63] K. Wu and M. Hella, "A 103-GHz voltage controlled oscillator with 28% tuning range and 4.2 dBm peak output power using SiGe BiCMOS technology," in *Proc. IEEE MTT-S Int. Microw. Symp.*, 2018, pp. 606–609, doi: [10.1109/MWSYM.2018.8439176](#).
- [64] A. Franceschin, D. Riccardi, and A. Mazzanti, "Ultra-low phase noise X-band BiCMOS VCOs leveraging the series resonance," *IEEE J. Solid-State Circuits*, vol. 57, no. 12, pp. 3514–3526, Dec. 2022, doi: [10.1109/JSSC.2022.3202405](#).
- [65] D. Riccardi, A. Franceschin, and A. Mazzanti, "16-core BiCMOS VCOs with phase noise down to -130 dBc/Hz at 1-MHz offset from 20 GHz," *IEEE Solid-State Circuits Lett.*, vol. 5, pp. 182–185, 2022, doi: [10.1109/LSSC.2022.3193236](#).
- [66] U. L. Rohde and A. K. Poddar, "Miniaturized VCOs arm configurable synthesizers," in *Proc. IEEE MTT-S Int. Microw. Symp.*, 2009, pp. 1281–1284, doi: [10.1109/MWSYM.2009.5165938](#).
- [67] A. P. S. Khanna and J. Buenrostro, "2.22 GHz low phase noise silicon bipolar YIG tuned oscillator using composite feedback," in *Proc. IEEE MTT-S Microw. Symp. Dig.*, 1992, vol. 3, pp. 1297–1299, doi: [10.1109/MWSYM.1992.188240](#).
- [68] W. Stein, F. Huber, S. Bildik, M. Aigle, and M. Vossiek, "An improved ultra-low-phase noise tunable YIG oscillator operating in the 6–12 GHz range," in *Proc. 47th Eur. Microw. Conf.*, 2017, pp. 767–770, doi: [10.23919/EuMC.2017.8230960](#).
- [69] A. A. Sweet and R. Parrott, "A wide band, low phase noise, differential YIG tuned oscillator," in *Proc. WAMICON*, 2014, pp. 1–3, doi: [10.1109/WAMICON.2014.6857764](#).
- [70] M. van Delden, N. Pohl, K. Aufinger, C. Baer, and T. Musch, "A low-noise transmission-type yttrium iron garnet tuned oscillator based on a SiGe MMIC and bond-coupling operating up to 48 GHz," *IEEE Trans. Microw. Theory Techn.*, vol. 67, no. 10, pp. 3973–3982, Oct. 2019, doi: [10.1109/TMTT.2019.2926293](#).

